Applied Surface Science 530 (2020) 147227

Contents lists available at ScienceDirect

Applied Surface Science

journal homepage: www.elsevier.com/locate/apsusc

Role of electron pressure in the problem of femtosecond laser action on metals

V.I. Mazhukin, M.M. Demin, A.V. Shapranov, A.V. Mazhukin

Keldysh Institute of Applied Mathematics, Moscow, Russia

ARTICLE INFO

Keywords:
Electronic pressure
Femtosecond laser action
Mathematical modeling

ABSTRACT

Based on the developed continuum model combining the description of nonequilibrium thermal, hydrodynamic, and electronic processes, a detailed study of the mechanisms of fs laser ablation of an Al film has been performed. The main feature of the mathematical formulation is the direct connection of the electron pressure gradient with the electric field strength, which allows us to study various ablation mechanisms within the framework of a unified mathematical model - fast non-thermal, determined by Coulomb forces and slow, realized in a hydrodynamic unloading wave. Modeling showed that excessive nonequilibrium pressure of collectivized electrons plays a leading role in the formation of a strong electric field at the metal-vacuum interface. This effect can be the basis of the Coulomb explosion in metals.

1. Introduction

The physics of the interaction of pulsed laser radiation with the near-surface region of condensed matter is the basis of pulsed laser ablation (PLA). Laser pulses of ultrashort (femto - picosecond) duration have the unique ability to release a certain amount of energy in solid targets. [1–3]. Since the duration of these pulses is shorter than the relaxation times of all the main processes, the released energy interacts only with the electrons, leaving the lattice cool for the time necessary to transfer the absorbed laser energy from the heated electrons to the lattice. For this reason, all processes induced by laser radiation in solid targets, including phase transformations that underlie laser ablation, proceed under nonequilibrium conditions. This leads to a fundamental difference in the behavior of physical processes in the irradiation zone from their equilibrium counterparts and is reflected in the properties of the irradiated materials.

Ultrashort laser ablation is one of the most promising areas for new laser applications, and opens up a wide range of new applications in the field of materials science [4,5], nanotechnology [6,7], biomedicine [8,9], etc.

A detailed study of the mechanisms of ultrashort laser ablation of metals and semiconductors remains a difficult task due to the wide variety of processes involved, which are characterized by strong spatio-temporal different scales. Therefore, a deep understanding of the processes initiated by ultrashort laser exposure is of not only practical, but also fundamental interest.

The determining factor for the processes under consideration is the time scale at which the energy of the laser pulse in the substance is released. This is evidenced by the experimentally measured [10 –12] using time-of-flight (TOF) mass spectrometry bimodal velocity and energy distribution of nanoparticles during femto- and picosecond laser ablation of metals (Al, Cu, Au, Fe) and semiconductors (Si) . The observed spectra with a two-peak particle distribution consist of two components - a high and low energy component. Obtaining clear bimodal structures with two different maxima in the distribution of nanoparticles in terms of velocities and energies ejected from the irradiated metal surfaces indicates that at least two different mechanisms contribute to ultrashort laser ablation. A distinctive feature of ultrashort laser action on metals, along with traditional thermal and hydrodynamic processes, is the presence of ultrafast electronic processes. The predominance of thermal and hydrodynamic processes is the basis of the mechanism of thermal ablation during which the main removal of matter occurs. This mechanism is slow, since in it the release and conversion of laser pulse energy occurs on a picosecond time scale.

Fast electronic processes are associated with electric fields and underlie the mechanism of fast non-thermal ablation, the implementation of which is carried out in a femtosecond time scale. Nonthermal ablation occurs near the threshold of main ablation and tends to remove hot electrons and accelerated ions from a thin surface layer. Fast electronic processes can lead to a Coulomb explosion (CE), a concept about the physical mechanisms of which for metals [13,14] and semiconductors [15,16,17] is not completely formulated and is a subject of considerable scientific interest [18 –20].

The possibilities of experimental studies are very limited, especially in the field of determining the dynamic characteristics of laser-induced nonequilibrium processes. The missing information can be supplemented by the results of theoretical studies and mathematical modeling. The success of mathematical modeling methods largely depends on the mathematical apparatus used: mathematical models and computational methods, the development of which is given constant

https://doi.org/10.1016/j.apsusc.2020.147227
Received 19 October 2019; Received in revised form 23 June 2020; Accepted 8 July 2020
Available online 13 July 2020
0169-4332/

attention [21 –25].

Currently, two classes of models are most widely used: continuum (macroscopic level) [26 –30] and atomistic (microscopic level) [31 –34]. Continual models and methods for solving them are more compact, have higher accuracy and a relatively small amount of computation. In atomistic models, classical or quantum systems of equations of motion are solved numerically, the number of which is equal to the number of particles (atoms, ions) that make up the sample. The price for this is a large amount of computation.

Note that at present, the behavior of the entire set of processes initiated by ultrashort pulsed laser radiation does not explain any of the traditional models.

In metals, the release of the absorbed fraction of the laser fluence in the electronic subsystem leads to the emergence of highly nonequilibrium states in which for a short time interval the temperature of the electronic subsystem can be by several orders of magnitude higher than the temperature of ions (atoms), $T_e \gg T_i$. For this reason, most theoretical studies have focused on the fundamental side of the transfer of thermal energy in the electronic subsystem and heat and energy exchange with the ionic subsystem. The determination of pressure under such nonequilibrium conditions encounters great difficulties [36] and certain contradictions. In particular, great difficulties arise in determining the electronic pressure and evaluating its effect on the properties of the ionic subsystem. Attempts were made to study its effect using blast force [37,38], which was obtained in [39], and the forces of interionic interaction for which special potentials of interparticle interaction were developed [36,40]. However, in general, the problem of electron pressure under conditions of strong unequality has remained insufficiently studied.

The purpose of this work is to present a new continual model of a hydrodynamic level that includes both physical mechanisms of ultrashort fs laser ablation in the description - fast non-thermal ablation and slow thermal one. Its use in the mathematical modeling in the study of nonequilibrium processes will allow us to build and explain the bimodal velocity distribution of nanoparticles in the framework of a single model, and also to determine the role of the pressure of electron Fermi gas of the metal in the Coulomb stage of the removal of fast particles from the target surface.

2. Physical and mathematical formulation

A laser beam with a Gaussian shape in the time coordinate t is incident on the surface of a metal target (Al) placed in vacuum. The laser wavelength is λ, maximum intensity Go, and duration τ. Part of the radiation is reflected by the surface ($0 < R < 1$, R is the reflection coefficient). The remaining radiation fraction $A = (1\text{-}R)$ is absorbed by the electronic component of the metal. The features of the problem under consideration are determined both by the regime of laser exposure and by the properties of the irradiated material (metal).

2.1. Hydrodynamic processes.

Ultrashort high-power laser action on materials is accompanied by powerful heat and mass transfer processes. Within the framework of the continuum approach, the most complete mathematical description of pulsed laser ablation in the long time scale, $t \gg \tau$, is carried out, as a rule, in the approximation of hydrodynamic models. They take into account the reaction of the irradiated material to changing density, pressure, and energy, as well as nonequilibrium effects associated with the violation of local thermodynamic equilibrium (LTE) [3,28,35,41]. The use of models of the hydrodynamic level suggests the presence of the processes with a characteristic propagation velocity of disturbances equal to the speed of sound in both subsystems - ionic and electronic υsi and υse. In this they differ from drift-diffusion models. Moreover, the difficulties observed in experimental studies of nonequilibrium processes also appear in the mathematical description. This primarily relates to the electronic subsystem and its interaction with the ionic subsystem.

As already noted, the duration of the action of ultrashort pulses is shorter than the relaxation times of all the main processes, and the absorbed energy of the laser pulse is released in the electronic component, leaving the lattice cold for the time necessary to transfer energy from heated electrons to the lattice. For this reason, all processes induced by laser radiation: electronic, thermal, hydrodynamic, including phase transformations, which underlie laser ablation, proceed under conditions of strong nonequilibrium, which must be adequately taken into account in the mathematical model. One of these effects is the action of the pressure of collectivized electrons in a metal under conditions when the temperatures of the electron and ion subsystems differ by tens of thousands of degrees. Taking into account the effect of the pressure of the electronic component leads to the necessity of constructing a hydrodynamic model, the solution of which will make it possible to fully reproduce the mode of not only slow thermal ablation in metal (Al), but also fast non-thermal one.

2.2. Electronic processes.

According to Sommerfeld's quantum–mechanical theory [42,43], metal consists of free collectivized electrons and heavy positively charged ions, which are considered immobile. Under normal conditions, free electrons are a degenerate electron gas obeying the Fermi - Dirac energy distribution. In the initial state, in the absence of external fields, it is assumed that the metal is in a state of thermodynamic equilibrium and quasineutrality. Collectivized electrons in the bulk of the metal, within the accuracy of an approximation of quasineutrality, have a constant density ρ_e and move freely through the lattice formed by bound ions. Ions also have a constant density ρ_i up to the boundary with vacuum $\times = L$, where the density of ions decreases stepwise to zero. Atoms and ions at the vacuum-metal interface (surface) exhibit other properties than atoms and ions in the bulk of a phase or material, since they are in a different environment. This is determined primarily by the fact that the surface of a solid metal is always charged, since it is formed by ions that make up the solid matter.

Under the influence of the pressure of the electronic component p_e, collectivized electrons are squeezed out of the metal surface in the direction of vacuum, which leads to a violation of quasineutrality and the appearance of an electric field. As a result, the presence of a surface charge leads to the formation of a thin double electric layer formed by two spatially separated layers of electric charges of different signs. The resulting electric field prevents electrons from going to infinity and helps establish electrostatic equilibrium, in which the positive charge of the metal surface is compensated by the negative charge of the electron cloud from the vacuum side.

An external action in the form of ultrashort superpowerful laser pulses on collectivized electrons can lead to a nonlinear response of the electronic component. This effect can underlie the mechanism of ultrafast (several hundred femtoseconds [13]) laser ablation with low density, which was experimentally observed in studies [10 –12]. Under suitable conditions, this same effect can lead to a Coulomb explosion.

3. Mathematical statement

The absorbed fraction of the laser pulse energy is spent on heating, phase transformations, and dynamic fragmentation of the irradiated target. A feature of the effect of ultrashort ultra-high-power laser radiation on metals is the high speed and volumetric nature of the energy release in the electronic component, which leads to a strong deviation from the state of local thermodynamic equilibrium. Together with thermodynamic nonequilibrium, in consideration it is necessary to take into account the kinetic nonequilibrium of high-speed heterogeneous phase transitions - melting/crystallization [29] and evaporation. The transfer of matter through phase boundaries under conditions of

volumetric energy release leads to the formation of metastable strongly superheated states resulting in appearance of homogeneous melting in the near-surface regions. The inclusion of these processes requires a description of the kinetics of phase transitions and the formulation of conservation laws at phase boundaries, which are hydrodynamic discontinuities.

3.1. Nonequilibrium hydrodynamic model

The most complete and consistent mathematical description of the processes under consideration requires the use of a 2-speed ($u_i \neq u_e$), 2-temperature ($T_i \neq T_e$) hydrodynamic model. In the present work, we use a simpler approximation of the single-speed ($u = u_i = u_e$) two-temperature ($T_i \neq T_e$) multi-front non-equilibrium hydrodynamic version of the Stefan problem [29], written in the domain of definition $(t \times x) = (0 < t < t_{end}) \times (0 < x < L)$ or solid and liquid phases. When using the equilibrium equations of state $p_a = p(\rho_a, T_a)$ and $\varepsilon_a = \varepsilon(\rho_a, T_a)$ for which the relations $\rho_a = \rho_e + \rho_i$, $T_a = T_e = T_i$ are satisfied, the model consists of hydrodynamic and energy equations describing the laws of conservation of mass, momentum and energy for the atomic subsystem (quantities with index a), and the law of conservation of the nonequilibrium part of energy for collectivized electrons. The model also contains the equation of laser radiation transfer.

The equation of motion is constructed in such a way that the gradient of the nonequilibrium electron pressure p_e^{ne} and the volumetric force of the electric field from the side of the double layer F^{ne} appearing in the near-surface metal - vacuum phase interface are explicitly shown as the source (the right side of the equation).

The nonequilibrium Coulomb force F^{ne} is determined from the solution of the problem of a double electric layer.

$$\left(\begin{array}{c} \frac{\partial \rho_a}{\partial t} + \frac{\partial (\rho_a u)}{\partial x} = 0 \\ \frac{\partial (\rho_a u)}{\partial t} + \frac{\partial (\rho_a u^2)}{\partial x} = -\frac{\partial (p_a + p_e^{ne})}{\partial x} + \rho_a F^{ne} \\ \frac{\partial (\rho_e \varepsilon_e^{ne})}{\partial t} + \frac{\partial (\rho_e \varepsilon_e^{ne} u)}{\partial x} = -\left(p_e^{ne} \frac{\partial u}{\partial x} + \frac{\partial W_e}{\partial x} + g(T_e)(T_e - T_a) + \frac{\partial G}{\partial x}\right) \\ \frac{\partial (\rho_a \varepsilon_a)}{\partial t} + \frac{\partial (\rho_a \varepsilon_a u)}{\partial x} = -\left(p_a \frac{\partial u}{\partial x} + \frac{\partial W_a}{\partial x} - g(T_e)(T_e - T_a)\right) \\ \frac{\partial G}{\partial x} + \alpha(T_e) G = 0 \end{array}\right)_{k=s,\ell} \quad (1)$$

$t > 0$,

$(L < x < \Gamma_{s\ell}(t)) \cup (\Gamma_{s\ell}(t) < x < \Gamma_{\ell v}(t))$,

$k = s, l$,

$$W_e = -\lambda_e(T_e, T_a)\frac{\partial T_e}{\partial x},$$

$$W_a = -\lambda_a(T_a)\frac{\partial T_a}{\partial x},$$

$$\rho_a = \rho_i + \rho_e, \quad \rho_e = z\frac{m_e}{m_i}\rho_i$$

where $x = \Gamma_{s\ell}(t)$, $x = \Gamma_{\ell v}(t)$ are moving phase fronts of melting-crystallization and evaporation, $x = L$ is the thickness of the target.

Accepted notation: the indices s, ℓ, v denote that the quantities belong respectively to the solid, liquid and vapor phases, e, i, a - to the electronic, ionic and atomic components. ρ, u, ε, T, p are the density, gas-dynamic velocity, internal energy, temperature and pressure of a substance, respectively, $\alpha(T_e)$ is the volume absorption coefficient, G is the laser radiation density, $C_{e,a}$, $\lambda_{e,a}$ are the specific heat and thermal conductivity coefficient, $g(T_e)$ is the electron–phonon coupling coefficient.

3.2. Equation of state

The equations of state of internal energy and pressure of the electronic subsystem are represented as the sum of the equilibrium and nonequilibrium components.

$$\begin{aligned} \varepsilon_e &= \varepsilon_e(\rho_e, T_e) = \varepsilon_e^{eq}(T_i) + \varepsilon_e^{ne}(T_i, T_e) \\ p_e &= p_e(\rho_e, T_e) = p_e^{eq}(T_i) + p_e^{ne}(T_i, T_e) \end{aligned} \quad (2)$$

The equilibrium atomic equations of state are represented as

$$\begin{aligned} p_a &= p(\rho_a, T_a) = p_i + p_e^{eq} \\ \rho_a \varepsilon_a &= \rho_i \varepsilon_i + \rho_e \varepsilon_e^{eq} \end{aligned} \quad (3)$$

In the electronic subsystem, the equations of state $\varepsilon_e = \varepsilon_e(\rho_e, T_e)$, $p_e = p_e(\rho_e, T_e)$ and electron density n_e can be expressed in terms of Fermi integrals of half-integer order $F_{k+1/2}(\eta)$ [44]

$$\varepsilon_e = T_e \frac{F_{3/2}}{F_{1/2}},$$

$$P_e = (n_e, T_e) = \frac{2}{3}(n_e < \varepsilon_e >),$$

$$n_e = g_0 \cdot (k_B T_e)^{3/2} F_{1/2}(\eta)$$

To calculate the Fermi – Dirac integrals, it is convenient to use approximation formulae [44,45]

$$F_{1/2}(\xi) = \frac{2}{3}\frac{1}{\xi^{3/2}}, \quad F_{3/2}(\xi) = \frac{\left(\xi^2 + \left(\frac{2}{5}\right)^2\right)^{1/2}}{\xi^{5/2}} \quad (4)$$

where $\xi = \frac{k_B T_e}{\varepsilon_F}$, $g_0 = \frac{2^{1/2} m^{3/2}}{\pi^2 h^3}$, m_e is the electron mass, ε_F is the Fermi energy, h is the Plank constant, η is the reduced chemical potential.

With account of (4), the equations of state $\varepsilon_e = \varepsilon_e(\rho_e, T_e)$, $p_e = p_e(\rho_e, T_e)$ take the form

$$p_e = n_e \varepsilon_F(n_e) \sqrt{\left(\frac{k_B T_e}{\varepsilon_F(n_e)}\right)^2 + \left(\frac{2}{5}\right)^2},$$

$$\varepsilon_e = \frac{3}{2}\frac{\varepsilon_F(n_e)}{m_e} \sqrt{\left(\frac{k_B T_e}{\varepsilon_F(n_e)}\right)^2 + \left(\frac{2}{5}\right)^2} \quad (5)$$

The equations given in [46] were used as equilibrium atomic equations of state.

In this model, all the thermophysical and optical characteristics of the degenerate Fermi gas and the condensed target phase are assumed to be temperature-dependent. For aluminum, these dependencies are taken from [29,47 –51].

3.3. Boundary conditions

The initial conditions are:

$t = 0$: $u(0, x) = 0$, $p(0, x) = 0$, $\rho(0, x) = \rho_0$, $T_e(0, x) = T_a(0, x) = T_0 = 293\,K$

The boundary conditions.

On the left boundary, the condition of zero mass and heat flux is written:

$x = 0$: $\rho_s u_s = 0$, $W_a = W_e = 0$

Heterogeneous melting/crystallization. At the moving interface $x = \Gamma_{s\ell}(t)$, the boundary conditions are formulated in the form of a nonequilibrium kinetic model of heterogeneous melting/crystallization [29,47] taking into account the strong thermodynamic nonequilibrium processes. Relations at the boundary are a system of nonlinear equations describing the laws of conservation of mass, momentum, and energy, supplemented by the dependence of the kinetic velocity $v_{s\ell}$ of the melting / crystallization front depending on overheating / supercooling of the surface $\Delta T_{s\ell} = T_{s\ell} - T_m(P_s)$ and the baric dependence of the melting temperature $T_m(P_s)$:

$x = \Gamma_{s\ell}(t)$: $\rho_s(u_s - v_\ell) = \rho_\ell(u_\ell - v_{s\ell})$

$$p_s + \rho_s(u_s - v_{s\ell})^2 = p_\ell + \rho_s(u_s - v_{s\ell})^2$$

$$\left(\lambda_a \frac{\partial T_a}{\partial x}\right)_s - \left(\lambda_a \frac{\partial T_a}{\partial x}\right)_\ell = L_m^{ne} \rho_s v_{s\ell} \quad (6)$$

$$\upsilon_{s\ell} = \upsilon_{s\ell}(\Delta T_{s\ell}) = \alpha(3k_B T_{s\ell}/m)^{1/2} \times \times\left(1 - \exp\left(\beta \frac{\mu L_m(T_m)}{R}\frac{\Delta T_{s\ell}}{T_m T_{s\ell}}\right)\right)$$

where

$T_m = T_m(p_a) = T_{m0} + \gamma p_a$ is the equilibrium melting curve,

$L_m(T_m(p_a)) = L_{m0} + \delta(T_m(p_a) - T_{m0})$ is the temperature dependence of the equilibrium heat of melting [48], $\Delta C_{ps} = (C_{ps} - C_{p\ell})$, $\Delta T_{s\ell} = (T_{s\ell} - T_m(p_a))$, $L_m^{ne} = L_m(T_m(p_s)) + \Delta C_{ps}\Delta T_{s\ell} + \frac{\rho_s + \rho_\ell}{\rho_s - \rho_\ell}\frac{(u_s - u_\ell)^2}{2}$ is the nonequilibrium heat of melting taking into account hydrodynamic effects, C_{ps}, $C_{p\ell}$, $\upsilon_{s\ell}$ are the specific heat of solid and liquid phases and kinetic velocity of the melting / crystallization front; T_{m0}, L_m are the equilibrium temperature and heat of melting. The parameters α, β, γ, δ are determined from the molecular modeling [29,47,48]. For Al they are equal to: α = 0.344, β = 5.01, γ = 6.44 10^{-3} K/bar, δ = 6.374 J/K/mole;

Upon transition through the phase boundary, the electronic component is assumed to be continuous with respect to the electron density ne and temperature Te:

$$\left(\lambda_e\frac{\partial T_e}{\partial x}\right)_s = \left(\lambda_e\frac{\partial T_e}{\partial x}\right)_\ell,\ T_{e,s} = T_{e,\ell}.$$

Heterogeneous evaporation. At the moving boundary, the surface evaporation model in the Knudsen layer approximation [52 –54] is used as boundary conditions, including three conservation laws and two additional kinetic relations, from which two of the three values on the outside of the Knudsen layer (T_υ, ρ_υ, u) are determined. The third quantity, usually the Mach number ($M = u / u_\ell$), is found from the solution of the equations of gas dynamics.

$$x = \Gamma_{k\upsilon}(t):\ \rho_k(u_k - \upsilon_{k\upsilon}) = \rho_\upsilon(u_\upsilon - \upsilon_{k\upsilon}),$$

$$p_{a,k} + \rho_k(u_k - \upsilon_{k\upsilon})^2 = p_{a,\upsilon} + \rho_\upsilon(u_\upsilon - \upsilon_{k\upsilon})^2$$

$$\left(\lambda_a\frac{\partial T_a}{\partial x}\right)_k - \left(\lambda_a\frac{\partial T_a}{\partial x}\right)_\upsilon = \rho_k(u_k - \upsilon_{k\upsilon})L_\upsilon^{ne} \quad (7)$$

$$\rho_\upsilon = \alpha_\rho(M)\rho_{sat}, \quad T_\upsilon = \alpha_T(M)T_k$$

$$p_{sat}(T_k) = p_b\exp\left(\frac{L_\upsilon\mu}{RT_b}\left(\frac{\Delta T_k}{T_k}\right)\right),$$

$$\rho_{sat} = p_{sat}(T_k)/(RT_k)$$

$$L_\upsilon^{ne} = L_\upsilon^{eq}(T_k) + \Delta C_{p\upsilon}(T_\upsilon - T_k) + \frac{\rho_k + \rho_\upsilon}{\rho_k - \rho_\upsilon}\frac{(u_k - u_\upsilon)^2}{2}$$

where $\Delta T_k = T_k - T_b$ ($p_{sat}(T_k)$), p_{sat}, ρ_{sat} are the pressure and density of saturated vapor, α_υ α_T are the kinetic coefficients, L_υ, L_υ^{ne} are equilibrium and non-equilibrium evaporation heat, p_b, T_b – steam pressure under normal conditions and equilibrium boiling point.

The boundary conditions for the electronic component and laser radiation are written as

$$-\lambda\frac{\partial T_e}{\partial x} = \sigma T_e^4$$

$$G(t) = (1 - R_k(T_e))G_0\exp(-(t/\tau)^2)$$

where σ is the Stefan-Boltzmann constant.

3.4. Model of double electric layer

The main difference between the mathematical statement of the double electric layer problem [55] and the drift–diffusion statements [18,19] is the direct connection of the electron pressure gradient with the electric field. This dependence follows from a macroscopic description of processes in a double electric layer. With the beginning of the action of laser radiation, the heated electrons come into motion with a certain thermal speed, which leads to a change in the concentration of electrons. The consequence of this is the emergence of a concentration gradient and, consequently, a gradient of electron pressure. In equilibrium, the forces of the electric field E acting on any arbitrary volume V are balanced by the pressure p acting on its surface S, which can be expressed by the following equality:

$$\int_V -en_e\vec{E}\,dV = \oint_S p d\vec{S} = \int_V grad\,p\,dV \quad (8)$$

After integration we obtain the following expressions

$$-en_e\vec{E} = grad\,p \quad (9)$$

In the one-dimensional case, (9) is written as

$$-en_eE_x = \frac{\partial p}{\partial x} \quad (10)$$

From the macroscopic expressions (8) - (10), using simple transformations, one can obtain the well-known Einstein relation underlying the drift–diffusion models [56]:

$$\frac{\mu_e}{D_e} = \frac{e}{k_B T_e}\ and\ \frac{\mu_i}{D_i} = \frac{ne}{k_B T_i}$$

Where e is the electron charge, μ_e, μ_i are the mobilities of electrons and ions, respectively, D_e, D_i are the diffusion coefficients of electrons and ions, respectively.

Following [55], we give a brief description of the mathematical model of a double electric layer. The mathematical formulation of the problem is reduced to two systems of equations, interconnected by a common boundary and conditionally called internal and external problems. The internal problem corresponds to processes in a metal with a positive charge ezn_i of ions uniformly distributed in a volume of $0 < x < L$ and a negative charge of collectivized electrons - en_e, which compensate for the positive charge in this region. The external problem corresponds to a region of an electron cloud with a negative charge, adjacent to the metal surface from the vacuum side, $L < x < \infty$. At the point $x = L$, there is a metal - degenerate gas of free electrons interface, on which the conjugation conditions of the internal and external problems are formulated.

Internal problem and External problem

$$\begin{cases} \frac{\partial p_i(x)}{\partial x} = zen_iE_x \\ \frac{\partial p_e(n_e)}{\partial x} = -en_eE_x \\ \varepsilon_0\frac{\partial E_x}{\partial x} = e(zn_i - n_e) \end{cases} \quad and \quad \begin{cases} \frac{\partial p_e(n_e)}{\partial x} = -en_eE_x \\ \varepsilon_0\frac{\partial E_x}{\partial x} = -en_e \end{cases} \quad (11)$$

$$0 < x < L \quad and \quad L < x < \infty$$

Boundary conditions:

$$x = 0:\quad n_e(x = 0) = zn_i, \quad E_x(x = 0) = 0$$

The condition of continuity at the metal surface:

$$x = \Gamma_{k\upsilon}(t):$$

$$n_e(x = \Gamma_{k\upsilon} -) = n_e(x = \Gamma_{k\upsilon} +)$$

$$E(x = \Gamma_{k\upsilon} -) = E(x = \Gamma_{k\upsilon} +)$$

Here n_e, E are the electron concentration and electric field strength; ε_0 is the dielectric constant; n_i, z are the concentration of ions in the condensed phase and the valence of the metal.

The input data for this problem are n_i, z, T_e. As a result of its solution, the spatial distributions of the electric field $E(x)$ and electron concentration $n_e(x)$ are obtained as the output.

To determine the force F^{ne}, the problem (11), at every time step of the solution of the problem (1), is solved for two values of the temperature: $T = T_e$ and $T = T_a$. For $T = T_e$ (it is assumed that $T_e \neq T_a$) the field strength is determined under the conditions of absence of LTE $E^{ne} = E(T_e)$ for the time for the electron gas temperature near the surface. The second calculation is performed at the equilibrium

temperature $T = T_a$ in order to determine the filed strength $E^{eq} = E(T_a)$ under the conditions of LTE.

Then specific force $F^{ne}(T_e,T_a)$, included in the problem (1) is calculated in the following way:

$$F^{ne}(T_e, T_a) = ze/m_a\ [E^{ne} - E^{eq}] \quad (12)$$

Here e is the electron charge, m_a is the mass of an ion (atom).

Moreover, in problem (1), one should use the boundary condition for the electronic component

$$\left.\frac{\partial p_e^{ne}}{\partial x}\right|_{x=\Gamma_{kv}} = 0 \quad (13)$$

since the transfer of momentum from electrons to heavy particles in the border region has already been taken into account by means of volumetric force F^{ne}.

Note that the undoubted advantage of the hydrodynamic representation of electronic processes is the ability to determine the electron beam as a whole, without detailing its components such as thermo-photo streams and the associated electron work function and space charge potential, since all these phenomena are taken into account in the total electron beam crossing the metal-vacuum boundary.

4. Computational algorithm

The numerical solution of the hydrodynamic model (1) - (7) is carried out by the finite-difference method [57], combined with the method of dynamic adaptation of the construction of computational grids [58–60]. The main feature of dynamic adaptation is the use of an arbitrary non-stationary coordinate system [61 –63]. This distinguishes this method from other approaches that use Euler and Lagrangian variables to construct computational grids. The use of an arbitrary non-stationary coordinate system allows one to carry out calculations with an arbitrary number of discontinuous solutions, such as shock waves and contact boundaries [64], propagating phase [60,65] and temperature fronts [66]. The method of dynamic adaptation is ideally suited to modeling the processes of fragmentation of condensed matter [28,50,51].

The algorithms of the formation of spallation of a single fragment are developed taking into account the fact that, within the framework of the continuum approach, it is not possible to represent the initial stage of nucleation, which in this paper is replaced by the introduction of a quasi-nuclus with a characteristic thickness of 0.5 nm. The criteria for the introduction of quasi- nuclei depend on the mode of laser action on the target. When thermal ablation is realized in the phase explosion mode, the introduction criterion is determined by the achievement of the maximum overheating of the metastable liquid phase in the region of the near-surface temperature maximum. In this case, saturated vapor is located between the two moving boundaries of the quasi- nuclus at the initial moment, and relations describing the kinetics of surface evaporation and condensation are used as boundary conditions at the boundaries. The process of introducing a quasi- nuclus is considered complete after the Mach number becomes positive on its evaporating walls, M > 0, [50,51].

Nonthermal laser ablation is realized, as a rule, under the influence of ultrashort femto-picosecond laser pulses using a Coulomb explosion [17 –19]. Another mechanism of ablation during ultrashort action is an unloading wave [28,67] with negative pressure, moving from the irradiated surface deep into the target.

If, in this case, a region appears in the substance that satisfies the spallation criteria in terms of negative pressure, time, and strain rate [68], then a quasi-nucleus characterizing the formation of a void in the target material can be introduced in this region. The spall pressure can be determined in two ways: at a strain rate of less than 10^{10} s $^{-1}$, the approach [68] is used, and at a higher speed, the spall pressure is determined from [67] using the constant spall time of 0.1 ps. Since during ablation in the unloading wave, the temperature in the fragmentation region is not too high (as a rule, it does not exceed the equilibrium boiling point, $T < T_b$), it is possible to simplify and without a significant deterioration in the accuracy of calculations, replace saturated vapor with vacuum and write down the boundary conditions for the two new boundaries as a contact condition condensed medium-vacuum.

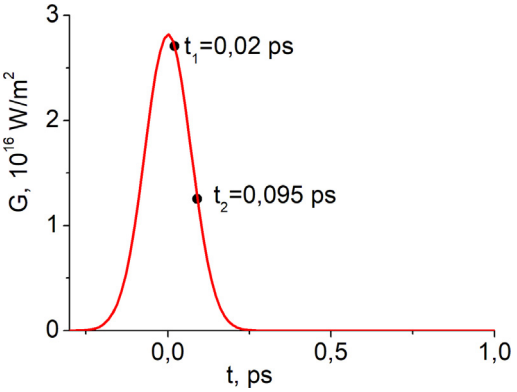

Fig. 1. The moments of the beginning of melting (t_1), maximum of the electron pressure and maximum of electron temperature (t_2) at the laser pulse shape.

The spalled fragment represents a new region in which a more detailed computational grid is automatically generated with condensation of the nodes to the both boundaries of the spalled part. Inside the new region, the velocity, density, and temperature were set to be the same as they were immediately before the split.

5. Analysis of results

Let us consider the option of exposing an aluminum target to an ultrashort laser pulse with a Gaussian time profile $G = G_0 exp(-(t/\tau)^2)$, where $-\infty < t < \infty$, $\tau = 0.1$ ps, $G_0 = 2.82 \times 10^{16}$ W/m^2, Fig. 1, fluence $F = 0.5$ J·cm^{-2} and wavelength $\lambda = 0.8$ μm, the surface reflectivity $R = 0.78$, $L = 2$ μm. The absorbed fraction of the pulse energy $(1-R)G(t)$ is completely released in the electronic component in the region, which dimensions are determined by the absorption coefficient $\ell \sim \alpha^{-1}$. The low heat capacity of the electron gas as compared to that of the lattice and the delayed energy exchange between the electron and ion subsystems contribute to the rapid heating of free electrons to a maximum temperature $T_{e,max} \approx 26\ 500$ K, Fig. 2, which is reached at the moment $t \approx 0.093$ ps, Fig. 1, while the maximum value of the lattice temperature T_{imax} is reached at ~ 2.6 ps, Fig. 2, that is, after the end of the laser pulse.

Maximum electron gas heating is limited by high electronic thermal conductivity $\lambda_e \gg \lambda_i$. In the ionic component, the delayed energy

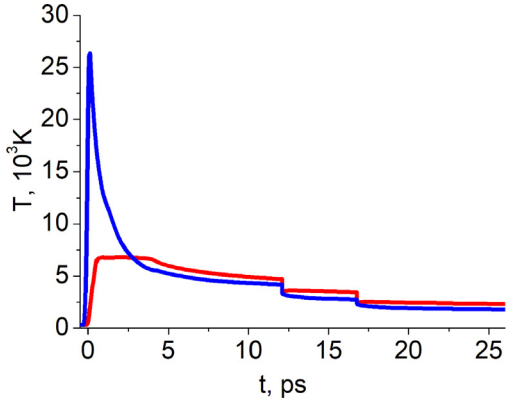

Fig. 2. Time dependence of the surface electron (T_e) and phonon (T_i) temperature.

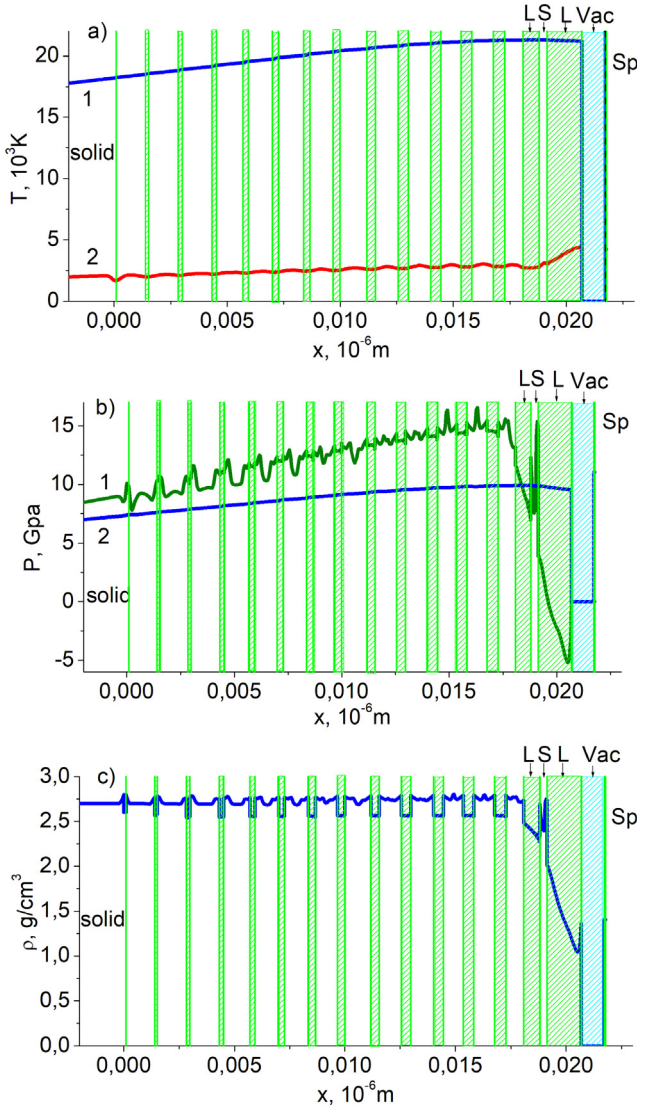

Fig. 3. Spatial profiles of main hydrodynamic properties at the moment $t \sim 0.3$ ps: (a) electron T_e (1) and ion T_i (2) temperature; (b) pressure (1) p_a, (2) p_e; (c) density ρ_a.

exchange between the subsystems leads to the fact that the melting of the superheated target surface begins on the falling side of the laser pulse $t \sim 0.02$ ps, Fig. 1 at the temperature ~ 1000 K, which is by ~ 70 K above the equilibrium melting temperature of aluminum T_m. Subsequently, the surface melting mechanism is rapidly replaced by a homogeneous one [28], the essence of which is as follows. Significant overheating of the melting surface and large spatial temperature gradients provide high propagation speeds $v_{s\ell}$ of the melting front $v_{s\ell} \sim$ (1–3) km/s. The powerful flow of matter through the interface $\Gamma_{s\ell}$, together with the continuing volumetric heating of the lattice due to the transfer of energy from the electronic component, leads to the formation of an overheated subsurface layer in the solid body with a temperature maximum, $T_{a,\max} > 1.4T_m(p_s)$. At the temperature maximum point, a quasi-nucleus of a new (liquid) phase is generated from which two fronts of the surface melting propagate in the opposite directions. The process is repeated while the volume heating of the lattice persists.

The features of the homogeneous melting process are illustrated at Fig. 3(a, b, c), which shows the spatial profiles of main hydrodynamic properties: temperature $T_i \approx T_e$, pressure p_a, p_e and density ρ_a under the conditions of multiple propagation of the melting fronts through the overheated solid phase at the moment $t \sim 0.3$ ps. These figures show the liquid phase as green, solid is white, vacuum as blue.

The rapid heating of free collectivized electrons by an ultrashort laser pulse in combination with a slowed-down energy exchange, determined by elastic electron–phonon collisions, which characteristic time τ_{ei} exceeds the characteristic relaxation times τe of the electron and ion τ_i subsystems $\tau_{ei} \gg \tau_i > \tau_e$, contribute to the formation of a state of strong thermodynamic nonequilibrium in the near-surface region metal-vacuum. In this area, characterized by the inequality $T_e \gg T_i$, the temperature gap between T_e and T_i at the surface is above 2×10^4 K, Fig. 2. An increase in the electron temperature T_e leads to an increase in the electron pressure p_e, which extrudes electrons toward the vacuum, which causes a charge separation near the metal-vacuum interface.

The emerging electric field seeks to maintain the quasi-neutral state of the system. Note that, in this case, the electron pressure acts only inside the electron gas, while the Coulomb force F^{ne} directly affects the ions from the side of the electron cloud. For the laser action regime under consideration, the maximum values of the electron pressure p_e and the electric field strength E_x on the target surface are reached on the descending branch of the laser pulse and are respectively $p_e \approx 15$ GPa, $E_x \approx 9 \times 10^9$ Vm^{-1} (Fig. 4), over the time, practically coinciding with the maximum of the electron temperature (Fig. 1).

The tensile effect of the Coulomb force manifests itself in the appearance of negative pressure p_a (of the order of 5 GPa) in the near-surface layer of the liquid, Fig. 3 (b). When the spallation criteria are reached [67,68], the surface layers of the substance are disrupted. In Fig. 4, vertical dashed lines mark the moments of the separation of the first five surface fragments by the Coulomb field. The thickness of the layer to be torn off is limited by the depth of the concentration inhomogeneity of free electrons. From the calculation of the structure of the double electric layer [55], the scale of the spatial concentration inhomogeneity of free electrons in the surface region of metals is of the order of 0.3–0,6 nm and weakly depends on T_e. The modeling showed that the thickness of the spalled layers are within the range 0.1–0.25 nm.

Fig 0.3(b) shows the formation of the negative (tensile) pressure p_a under the influence of the Coulomb force in the near-surface liquid region at the moment $t = 0.3$ ps, when the spallation of the first layer already occurred. A similar situation of negative pressure formation in the near-surface region is repeated before the spallation of the next thin layer. All spalled layers have a high speed $U \approx$ (8–14)km s^{-1}, Fig. 5(d).

After the end of the laser pulse, over time, under the influence of spatial heat transfer of electron energy and electron–phonon energy

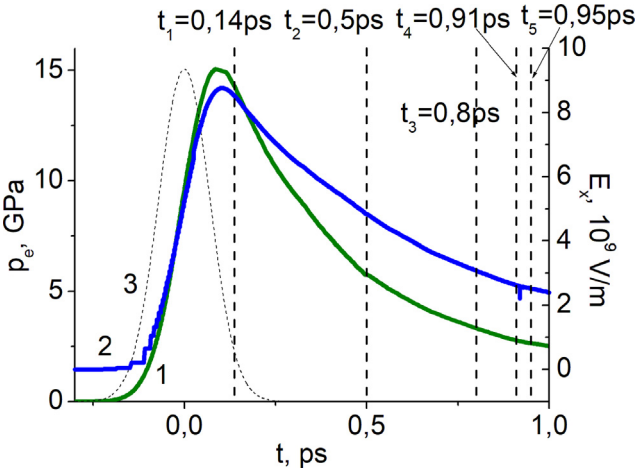

Fig. 4. Time dependence of electron pressure (1) (green), electric field strength (2) (blue), profile of the laser pulse (3). (t_1-t_5) are the moments of spallation of the first 5 liquid layers. (For interpretation of the references to colour in this figure legend, the reader is referred to the web version of this article.)

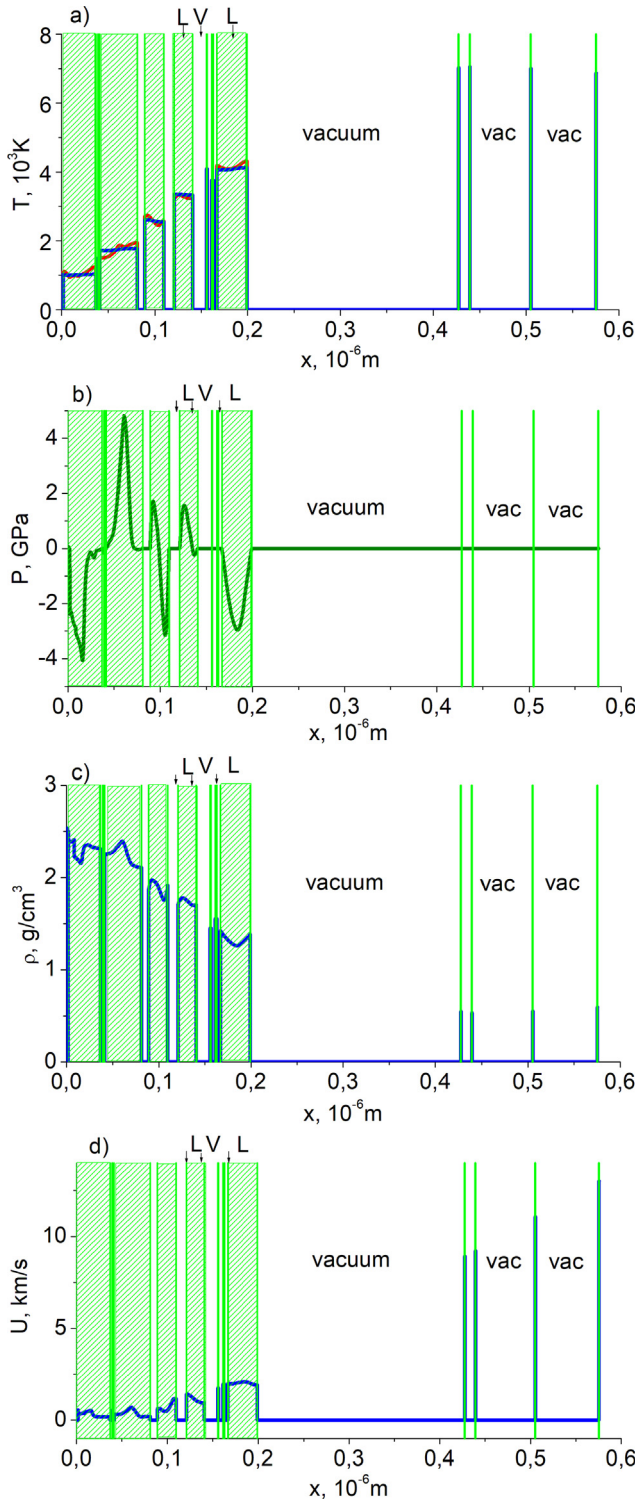

Fig. 5. Spatial distributions of the main properties of the spalled fragments: (a) temperature *T(x);* (b) pressure *p(x);* (c) density ρ(*x*); (d) velocity of expansion of the spalled layers.

transfer, the degree of thermodynamic nonequilibrium rapidly decreases. This is manifested in the equalization of the temperatures $T_e \approx T_i$ and the pressures $p_e \approx p_e^{eq}$, $p_a \approx p_i + p_e^{eq}$ and the disappearance of the excess Coulomb force $F^{ne}(T_e, T_a) = 0$ generated by the nonequilibrium electron pressure p_e^{ne}. A decrease in thermodynamic nonequilibrium entails a change in the main mechanisms of ablation. The mechanism of fast non-thermal ablation associated with electric fields is replaced by a mechanism of relatively slow thermal ablation, where the main role is played by thermal and hydrodynamic processes.

By the time $t \approx 12$ ps, the melting mechanism changes. The process of homogeneous melting of an overheated solid region with many local melting fronts ends. The entire superheated region turns into a liquid with a size of ~ 110 nm and one common solid–liquid interface. The melting process goes into a heterogeneous stage in which the common melting front runs along an overheated solid phase ($T \approx 1100$ K) at a speed of $v_{sl} \approx 1$ km/s. But for the introduction of quasi-nuclei of a new phase, such an overheating of the solid phase is insufficient.

By this time, the compression wave of the substance, caused by the rapid release of laser pulse energy, is followed by a hydrodynamic discharge wave with negative pressure, which leads to the appearance of the first spallation of a liquid fragment 33 nm thick. A series of spalls follows, the largest of them with sizes of 19 nm, 20 nm, 42 nm appear, respectively, at times $t_i \approx 16$ ps, 20 ps, 29 ps.

Between them is a series of small spalls with a number of ~ 10 with characteristic sizes of 1–2 nm. Fig. 5(a - d) show spatial profiles of the main properties of the spalled fragments: temperature *T(x),* pressure *p (x),* density ρ(*x*) and velocity *U(x)*. For comparison, the fragments that had separated earlier at the stage of high-speed ablation are also placed in the same figures.

Modeling showed that the total amount of spalled material at the stage of rapid non-thermal ablation is equivalent to 0.23 nm of solid phase. At the stage of slow thermal ablation, the removal of matter is equivalent to 78 nm of the solid phase. The expansion speeds of the spalled fragments under the influence of Coulomb are in the range of 8–12 km/s, while in the unloading wave the typical velocities do not exceed 2 km/s.

The results obtained are in good agreement with experimental observations of the bimodal distributions of nanoparticles by the energies given in [10 –12].

6. Conclusion

Ultrashort fs laser action on metals indicated the need to improve the mathematical models taking into account new processes in the target and the effects that did not play a significant role in other modes of laser action. One of these unaccounted effects is the influence of the pressure of collectivized electrons in a metal under conditions of strong thermodynamic nonequilibrium.

A mathematical continuous model is proposed combining a description of nonequilibrium thermal, hydrodynamic, and electronic processes. Its implementation is carried out in the framework of a one-dimensional in space, one-speed and two temperature approximations supplemented by models of a double electric layer, homogeneous melting and two temperature equations of state.

The main feature of the proposed model, in contrast to the previously used drift–diffusion mathematical formulations, is the use of the hydrodynamic approximation to describe electronic processes in a double electric layer. The direct connection of the electron pressure gradient with the electric field strength allows one to take into account and determine the nonequilibrium force acting on the atomic subsystem in the explicit form in the hydrodynamic model (1). Direct connection of the gradient of electron pressure with the electric field allows one to directly connect the hydrodynamic effects of the electronic component with the electric ones.

Modeling of the fs-laser action on the Al film made it possible to establish the presence of two pulsed laser ablation mechanisms:

- fast non-thermal, in which the generation of nanoparticles with a high expansion speed is carried out by the nonequilibrium Coulomb force of the double electric layer;
- slow thermal, in which the removal of matter occurs in a hydrodynamic unloading wave with negative pressure.

The results obtained are in good agreement with experimental observations of bimodal energy distributions of nanoparticles.

Excessive nonequilibrium pressure of collectivized electrons plays a leading role in the formation of a strong electric field at the metal - vacuum interface. This effect can be the basis of the Coulomb explosion in metals.

Representation of electronic processes in the hydrodynamic approximation allows us to represent the whole electron flow crossing the metal-vacuum interface. And by this, to exclude from consideration individual components of the total flux, such as thermionic electron flux (Richardson-Dushman formula), multiphoton emission, and related electron work function and charge potential.

If necessary, most of these quantities can be determined from the hydrodynamic formulation of the double electric layer, which the authors intend to fulfill in their next publications.

CRediT authorship contribution statement

V.I. Mazhukin: Conceptualization, Methodology. **M.M. Demin:** Software. **A.V. Shapranov:** Visualization, Investigation. **A.V. Mazhukin:** Investigation.

Declaration of Competing Interest

The authors declare that they have no known competing financial interests or personal relationships that could have appeared to influence the work reported in this paper.

Acknowledgements

This work was supported by Russian Science Foundation (project No. 18-11-00318).

References

[1] E.G. Gamaly, The physics of ultra-short laser interaction with solids at non-relativistic intensities, Phys. Rep. 508 (4–5) (2011) 91–243, https://doi.org/10.1016/j.physrep.2011.07.002.
[2] D. Von der Linde, K. Sokolowski-Tinten, J. Bialkowski, Laser-solid interaction in the femtosecond time regime, Appl. Surf. Sci. 109 (1997) 1–10.
[3] A.V. Mazhukin, V.I. Mazhukin, M.M. Demin, Modeling of femtosecond ablation of aluminum film with single laser pulses, Appl. Surf. Sci. 257 (2011) 5443–5446, https://doi.org/10.1016/j.apsusc.2010.11.154.
[4] Subhash Chandra Singh, Haibo Zeng, Chunlei Guo, W. Cai, Nanomaterials: Processing and Characterization with Lasers, Wiley-VCH, Weinheim, 2012.
[5] S. Bashir, M.S. Rafique, W. Husinsky, Surface topography (nano-sized hillocks) and particle emission of metals, dielectrics and semiconductors during ultra-short-laser ablation: Towards a coherent understanding of relevant processes, Appl. Surf. Sci. 255 (20) (2009) 8372–8376, https://doi.org/10.1016/j.apsusc.2009.05.090.
[6] J. Cheng, C.-S. Liu, S. Shang, D. Liu, W. Perrie, G. Dearden, K. Watkins, A review of ultrafast laser materials micromachining, Opt. Laser Technol. 46 (2013) 88–102.
[7] K. Ahmmed, C. Grambow, A. Kietzig, Fabrication of Micro/Nano Structures on Metals by Femtosecond Laser Micromachining, Micromachines 5 (4) (2014) 1219–1253, https://doi.org/10.3390/mi5041219.
[8] A. Muñoz-Noval, Silicon-based hybrid luminescent/magnetic porous nanoparticles for biomedical applications, J. Nanophoton. 5 (1) (2011) 051505, , https://doi.org/10.1117/1.3549739.
[9] E. Fadeeva, V.K. Truong, M. Stiesch, B.N. Chichkov, R.J. Crawford, J. Wang, E.P. Ivanova, Bacterial retention on superhydrophobic titanium surfaces fabricated by femtosecond laser ablation, Langmuir 27 (2011) 3012–3019.
[10] S. Amoruso, X. Wang, C. Altucci, C. de Lisio, M. Armenante, R. Bruzzese, N. Spinelli, R. Velotta, Double-peak distribution of electron and ion emission profile during femtosecond laser ablation of metals, App. Surf. Sci. 186 (1–4) (2002) 358–363, https://doi.org/10.1016/S0169-4332(01)00679-1.
[11] H. Dachraoui, W. Husinsky, G. Betz, Ultra-short laser ablation of metals and semiconductors: evidence of ultra-fast Coulomb explosion, Appl. Phys. A 83 (2) (2006) 333–336, https://doi.org/10.1007/s00339-006-3499-y.
[12] H. Dachraoui, W. Husinsky, Fast electronic and thermal processes in femtosecond laser ablation of Au, Appl. Phys. Lett. 89 (2006) 104102, , https://doi.org/10.1063/1.2338540.
[13] A. Vella, B. Deconihout, L. Marrucci, E. Santamato, Femtosecond Field Ion Emission by Surface Optical Rectification. Phys. Rev. Lett., 99(4) (2007) 046103-4. doi:10.1103/physrevlett.99.046103.
[14] Shuchang Lia, Suyu Lia, Fangjian Zhanga, Dan Tiana, He Lia, Dunli, Liua, Yuanfei Jianga, Anmin Chena, Mingxing Jina. Possible evidence of Coulomb explosion in the femtosecond laser ablation of metal at low laser fluence, App. Surf. Sci. 355 (2015) 681–685.
[15] Hai-Ping Cheng, J. D. Gillaspy. Nanoscale modification of silicon surfaces via Coulomb explosion. Phys. Rev. B, 55(4) (1997-II) 2628 - 2636. doi:10.1103/PhysRevB.55.2628.
[16] R. Stoian, A. Rosenfeld, I.V. Hertel, N.M. Bulgakova, E.E. Campbell, Comment on "Coulomb explosion in femtosecond laser ablation of Si(111)", Appl. Phys. Lett. 82 (4190) (2003) 694–695, https://doi.org/10.1063/1.1771817.
[17] W.G. Roeterdink, L.B.F. Juurlink, O.P.H. Vaughan, J. Dura Diez, M. Bonn, A.W. Kleyn, Coulomb explosion in femtosecond laser ablation of Si(111), App. Phys. Lett. 82 (23) (2003) 4190–4192, https://doi.org/10.1063/1.1580647.
[18] N.M. Bulgakova, R. Stoian, A. Rosenfeld, W. Marine, E.E. Campbell. A general continuum approach to describe fast electronic transport in pulsed laser irradiated materials: the problem of Coulomb explosion. Proc. SPIE 5448, High-Power Laser Ablation V, (20 September 2004). doi:10.1117/12.548823.
[19] Sh.a. Tao, Wu. Benxin, The effect of emitted electrons during femtosecond laser–metal interactions: A physical explanation for coulomb explosion in metals, App. Surf. Sci. 298 (2014) 90–94.
[20] M.V. Shugaev, C. Wu, O. Armbruster, A. Naghilou, N. Brouwer, D.S. Ivanov, L.V. Zhigilei, Fundamentals of ultrafast laser–material interaction, MRS Bulletin 41 (12) (2016) 960–968, https://doi.org/10.1557/mrs.2016.274.
[21] A.V. Mazhukin, O.N. Koroleva, V.I. Mazhukin, A.V. Shapranov, Continual and molecular dynamics approaches in determining thermal properties of silicon, Proceedings Volume 10453, Third International Conference on Applications of Optics and Photonics; 104530Y, 2017, https://doi.org/10.1117/12.2271999.
[22] V.S. Belyaev, G.S. Bisnovatyi-Kogan, A.I. Gromov, B.V. Zagreev, A.V. Lobanov, A.P. Matafonov, S.G. Moiseenko, O.D. Toropina, Numerical Simulations of Magnetized Astrophysical Jets and Comparison with Laboratory Laser Experiments Astronomicheskii Zhurnal 95 (3) (2018) 171–192.
[23] V.I. Mazhukin, A.V. Shapranov, E.N. Bykovskaya, Comparative analysis of the quality of two-and three-layer difference schemes of the second order, Mathematica Montisnigri 42 (2018) 31–51.
[24] D.S. Ivanov, L.V. Zhigilei, Combined atomistic-continuum modeling of short-pulse laser melting and disintegration of metal films, Phys. Rev. B 68 (2003) 064114.
[25] M.V. Shugaev, C.Y. Shih, E.T. Karim, C. Wu, L.V. Zhigilei, Generation of nanocrystalline surface layer in short pulse laser processing of metal targets under conditions of spatial confinement by solid or liquid overlayer, App. Surf. Sci. 417 (2017) 54–63.
[26] M.D. Shirk, P.A. Molian, A review of ultrashort pulsed laser ablation of materials, J. Laser Appl. 10 (1998) 18–28.
[27] Xin Zhao, Yung C. Shin, Femtosecond laser ablation of aluminum in vacuum and air at high laser intensity, Appl. Surf. Sci. 283 (2013) 94–99.
[28] V.I. Mazhukin, M.M. Demin, A.V. Shapranov, High-speed laser ablation of metal with pico- and subpicosecond pulses, Appl. Surf. Sci. 302 (2014) 6–10.
[29] V.I. Mazhukin, A.V. Shapranov, A.V. Mazhukin, O.N. Koroleva, Mathematical formulation of a kinetic version of Stefan problem for heterogeneous melting/crystallization of metals, Mathematica Montisnigri 36 (2016) 58–77.
[30] Xiao Jia, Xin Zhao, Numerical study of material decomposition in ultrafast laser interaction with metals, App. Surf. Sci. 463 (2019) 781–790.
[31] C.R. Cheng, X.F. Xu, Mechanisms of decomposition of metal during femtosecond laser ablation, Phys. Rev. B 72 (2005) 165415.
[32] D. Bouilly, D. Perez, L.J. Lewis, Damage in materials following ablation by ultrashort laser pulses: A molecular-dynamics study, Phys. Rev. B 76 (2007) 184119.
[33] V.I. Mazhukin, A.A. Samokhin, A.V. Shapranov, M.M. Demin. Modeling of thin film explosive boiling - surface evaporation and electron thermal conductivity effect. Mater. Res. Express, 2-1 (2015) 016402 (1-9). doi:10.1088/2053-1591/2/1/016402.
[34] V.I. Mazhukin, A.A. Samokhin, M.M. Demin, A.V. Shapranov, Explosive boiling of metals upon irradiation by a nanosecond laser pulse, Quantum Electronics 44–4 (2014) 283–285.
[35] C.Y. Shih, R. Streubel, J. Heberle, A. Letzel, M.V. Shugaev, C. Wu, L.V. Zhigilei, Two mechanisms of nanoparticle generation in picosecond laser ablation in liquids: the origin of the bimodal size distribution, Nanoscale 10 (15) (2018) 6900–6910, https://doi.org/10.1039/c7nr08614h.
[36] B. Chimier, V.T. Tikhonchuk, L. Hallo, Effect of pressure relaxation during the laser heating and electron–ion relaxation stages, Appl. Phys. A 92 (4) (2008) 843–848, https://doi.org/10.1007/s00339-008-4578-z.
[37] Vladimir V. Stegailov, Sergey V. Starikov, Genri E. Norman, Atomistic simulation of laser ablation of gold: the effect of electronic pressure, AIP Conf. Proc. 1426 (2012) 905–908, https://doi.org/10.1063/1.3686424.
[38] J.K. Chen, D.Y. Tzou, J.E. Beraun, A semiclassical two-temperature model for ultrafast laser heating, Int. J Heat. Mass. Tran. 49 (2006) 307–316.
[39] L.A. Falkovsky, E.G. Mishchenko, Electron-lattice kinetics of metals heated by ultrashort laser pulses, JETP 88 (1999) 84–88.
[40] S. Khakshouri, D. Alfè, D.M. Duffy, Development of an electron-temperature-dependent interatomic potential for molecular dynamics simulation of tungsten under electronic excitation, Phys. Rev. B 78 (2008) 224304, , https://doi.org/10.1103/PhysRevB.78.224304.
[41] V.I. Mazhukin, M.G. Lobok, B.N. Chichkov, Modeling of fast phase transitions dynamics in metal target irradiated by pico and femto second pulsed laser, App. Surf. Sci. 255–10 (2008) 5112–5115, https://doi.org/10.1016/j.apsusc.2008.08.014.
[42] G. Bete, A. Sommerfeld, Elektronnaya teoriya metallov, ONTI Glavnaya redakciya tekhniko-teoreticheskoj literatury, Moskva, 1938.
[43] N.W. Ashcroft and N.D. Mermin, Solid State Physics, W. B. Saunders Co., 1976.
[44] V.I. Mazhukin, Kinetics and Dynamics of Phase Transformations in Metals under Action of Ultra-Short High-Power Laser Pulses, in: I. Peshko (Ed.), Laser Pulses –

Theory, Technology, and Applications, InTech, Croatia, 2012, pp. 219–276.
[45] Ju.V. Martynenko, Ju.N. Javlinskii, Okhlazhdenie ehlektronnogo gaza metalla pri vysokojj temperature, DAN SSSR 270 (1) (1983) 88–91.
[46] I.V. Lomonosov, Multi-phase equation of state for aluminum, Laser and Particle Beams 25 (2007) 567–584.
[47] V.I. Mazhukin, A.V. Shapranov, V.E. Perezhigin, O.N. Koroleva, A.V. Mazhukin, Kinetic Melting and Crystallization Stages of Strongly Superheated and Supercooled Metals, Mathematical Models and Computer Simulations 9–4 (2017) 448–456, https://doi.org/10.1134/S2070048217040081.
[48] V.I. Mazhukin, A.V. Shapranov, V.E. Perezhigin, Matematicheskoe modelirovanie teplofizicheskikh svoi'stv, protcessov nagreva i plavleniia metallov metodom molekuliarnoi' dinamiki, Mathematica Montisnigri 24 (2012) 47–65.
[49] V.I. Mazhukin, A.V. Mazhukin, O.N. Koroleva, Optical properties of electron Fermi-gas of metals at arbitrary temperature and frequency, Laser Physics 19 (5) (2009) 1179–1186.
[50] V.I. Mazhukin, A.V. Shapranov, M.M. Demin, A.V. Mazhukin, Modeling of dynamics of nanosecond laser ablation in phase explosion regime, Proc. of SPIE 10453 (2017) 104530X, https://doi.org/10.1117/12.2271981.
[51] V.I. Mazhukin, A.V. Mazhukin, M.M. Demin, A.V. Shapranov, Nanosecond laser ablation of target Al in a gaseous medium: explosive Boiling, App. Phys. A, 124 (2018) 237(1-10). doi:10.1007/s00339-018-1663-9.
[52] D. Croat, An Application of Kinetic Theory to the Problems of Evaporation and Sublimation of Monoatimic Cases, J. Math. Phys. 15 (1936) 1–54.
[53] V.I. Mazhukin, A.A. Samokhin, Boundary conditions for gas-dynamical modeling of evaporation processes, Mathematica Montisnigri 24 (2012) 8–17.
[54] Yuri Zudin, Non-Equilibrium Evaporation, Condensation Processes, Analytical Solutions, Mathematical Engineering, Springer International Publishing (2019), https://doi.org/10.1007/978-3-319-67306-6.
[55] V.I. Mazhukin, A.V. Shapranov, A.V. Mazhukin, The structure of the electric double layer at the metal-vacuum interface, Mathematica Montisnigri. 44 (2019) 110–121, https://doi.org/10.20948/mathmon-2019-44-9.
[56] E.M. Lifshicz, L.P. Pitaevskij, Teoreticheskaya fizika. Fizicheskaya kinetika, t.10, M., Nauka, 1979.
[57] A.A. Samarskii, The theory of difference schemes, Marcel Dekker Inc, New York – Basel, 2001.
[58] N.A. Dar'in, V.I. Mazhukin, Ob odnom podhode k postroeniiu adaptivny'kh raznostny'kh setok. Doclady' AN SSSR, 298(1) (1988) 64–68.
[59] N.A. Dar'in, V.I. Mazhukin, A.A. Samarskii, Konechno-raznostny'i' metod resheniia odnomerny'kh uravnenii' gazovoi' dinamiki na adaptivny'kh setkakh, Doclady' AN SSSR, 302(5) (1988) 1078-1081.
[60] V.I. Mazhukin, I. Smurov, C. Dupuy, D. Jeandel, Simulation of Laser Induced Melting and Evaporation Processes in Superconducting, J. Numerical Heat Transfer, Part A 26 (1994) 587–600.
[61] V.I. Mazhukin, O. Kastel'yanos, A.A. Samarskii, A.V. Shapranov, Metod dinamicheskoi' adaptatcii dlia nestatcionarny'kh zadach s bol'shimi gradientami. Matematicheskoe modelirovanie, 5(4) (1993) 32–56.
[62] V.I. Mazhukin, M.M. Demin, A.V. Shapranov, I. Smurov, The method of construction dynamically adapting grids for problems of unstable laminar combustion, Numerical Heat Transfer, Part B: Fundamentals 44 (4) (2003) 387–415.
[63] A.V. Mazhukin, V.I. Mazhukin, Dynamic Adaptation for Parabolic Equations, Computational Mathematics and Mathematical Physics 47 (11) (2007) 1833–1855, https://doi.org/10.1134/S0965542507110097.
[64] P.V. Breslavskii, V.I. Mazhukin, Dynamically Adapted Grids for Interacting Discontinuous Solutions, Computational Mathematics and Mathematical Physics 47 (4) (2007) 687–706, https://doi.org/10.1134/S0965542507040124.
[65] V. Mazhukin, M. Chuiko, Solution of the multi-interface Stefan problem by the method of dynamic adaptation, J. Comput. Methods Appl. Math. 2 (3) (2002) 283–294.
[66] P.V. Breslavskiy, A.V. Mazhukin, O.N. Koroleva, Simulation of the dynamics of plasma expansion, the formation and interaction of shock and heat waves in the gas at the nanosecond laser irradiation, Mathematica Montisnigri 33 (2015) 5–24.
[67] D.E. Grady, The spall strength of condensed matter, J. of Mech. and Phys. of Solids 36 (3) (1988) 353–384.
[68] Maxim V. Shugaev, Leonid V. Zhigilei, Thermodynamic analysis and atomistic modeling of subsurface cavitation in photomechanical spalation, Comput. Mater. Sci. 166 (2019) 311–317, https://doi.org/10.1016/j.commatsci.2019.05.017.